frontiers | Frontiers in Cell and Developmental Biology

TYPE Original Research
PUBLISHED 16 February 2023
DOI 10.3389/fcell.2023.1113675

OPEN ACCESS

EDITED BY
Arjun Singh,
Memorial Sloan Kettering Cancer Center, United States

REVIEWED BY
Caroline Wee,
Institute of Molecular and Cell Biology (A*STAR), Singapore
Akira Muto,
Toho University, Japan

*CORRESPONDENCE
Y. Albert Pan,
yapan@vtc.vt.edu

SPECIALTY SECTION
This article was submitted to Molecular and Cellular Pathology, a section of the journal Frontiers in Cell and Developmental Biology

RECEIVED 01 December 2022
ACCEPTED 30 January 2023
PUBLISHED 16 February 2023

CITATION
Ma M, Brunal AA, Clark KC, Studtmann C, Stebbins K, Higashijima S-i and Pan YA (2023), Deficiency in the cell-adhesion molecule *dscaml1* impairs hypothalamic CRH neuron development and perturbs normal neuroendocrine stress axis function.
Front. Cell Dev. Biol. 11:1113675.
doi: 10.3389/fcell.2023.1113675

Deficiency in the cell-adhesion molecule *dscaml1* impairs hypothalamic CRH neuron development and perturbs normal neuroendocrine stress axis function

Manxiu Ma[1], Alyssa A. Brunal[1,2], Kareem C. Clark[1], Carleigh Studtmann[1,2], Katelyn Stebbins[1,2,3], Shin-ichi Higashijima[4] and Y. Albert Pan[1,5,6]*

[1]Fralin Biomedical Research Institute at Virginia Tech Carilion, Virginia Tech, Roanoke, VA, United States, [2]Translational Biology Medicine and Health Graduate Program, Virginia Tech, Blacksburg, VA, United States, [3]Virginia Tech Carilion School of Medicine, Roanoke, VA, United States, [4]National Institutes of Natural Sciences, Exploratory Research Center on Life and Living Systems, National Institute for Basic Biology, Okazaki, Aichi, Japan, [5]Department of Biomedical Sciences and Pathobiology, Virginia-Maryland College of Veterinary Medicine, Virginia Tech, Blacksburg, VA, United States, [6]Department of Psychiatry and Behavioral Medicine, Virginia Tech Carilion School of Medicine, Roanoke, VA, United States

The corticotropin-releasing hormone (CRH)-expressing neurons in the hypothalamus are critical regulators of the neuroendocrine stress response pathway, known as the hypothalamic-pituitary-adrenal (HPA) axis. As developmental vulnerabilities of CRH neurons contribute to stress-associated neurological and behavioral dysfunctions, it is critical to identify the mechanisms underlying normal and abnormal CRH neuron development. Using zebrafish, we identified *Down syndrome cell adhesion molecule like-1* (*dscaml1*) as an integral mediator of CRH neuron development and necessary for establishing normal stress axis function. In *dscaml1* mutant animals, hypothalamic CRH neurons had higher *crhb* (the CRH homolog in zebrafish) expression, increased cell number, and reduced cell death compared to wild-type controls. Physiologically, *dscaml1* mutant animals had higher baseline stress hormone (cortisol) levels and attenuated responses to acute stressors. Together, these findings identify *dscaml1* as an essential factor for stress axis development and suggest that HPA axis dysregulation may contribute to the etiology of human *DSCAML1*-linked neuropsychiatric disorders.

KEYWORDS

HPA (hypothalamic-pituitary-adrenal) axis, zebrafish, CRH neuron, hypothalamus, development

Introduction

The hypothalamic corticotropin-releasing hormone (CRH)-expressing neurons are the central regulators of the neuroendocrine stress response pathway, known as the hypothalamic-pituitary-adrenal (HPA) axis in mammals or the hypothalamic-pituitary-interrenal (HPI) axis in fish (Denver, 2009). Upon exposure to environmental disturbances

(i.e., stressors), stress-related neural inputs converge on hypothalamic CRH neurons to activate a hormonal cascade that ultimately leads to the release of glucocorticoids, which broadly affects cognitive, affective, metabolic, and immune functions (Spencer and Deak, 2017; McEwen and Akil, 2020).

The development of CRH neurons has profound effects on the function of the HPA and HPI axis (collectively referred to as the stress axis). Developmental perturbations of CRH neurons, particularly in early-life periods, lead to long-term changes in CRH neuron function (Regev and Baram, 2014). Additionally, rodent models demonstrate that dysregulation of CRH neurons increases anxiety- and depressive-like phenotypes (Keen-Rhinehart et al., 2009; Kolber et al., 2010). These studies underscore the need to identify the genes and molecules mediating CRH-neuron development and determine how developmental perturbations affect stress axis function.

During early development, hypothalamic CRH neurons are generated from progenitors in the ventral diencephalon (Alvarez-Bolado, 2019; Nagpal et al., 2019; Placzek et al., 2020). Secreted factors including FGF10, SHH, BMPs, and Nodal first define the anterior-dorsal hypothalamic domain; within this domain, CRH neurons are progressively specified by a combination of key transcription factors, including Fezf2, Otp, Sim1, Arnt2, and Brn2. Once specified, CRH neurons undergo further differentiation, such as neuronal morphogenesis, synaptogenesis, epigenetic programming, and cell death, to establish a functional stress-responsive neural circuit. These later stages of neuronal differentiation are shaped by intercellular interactions mediated by membrane-localized cell-adhesion molecules (Moreland and Poulain, 2022). The specific cell-adhesion molecules that mediate developmental signaling in CRH neurons, however, are still unknown.

To address this knowledge gap, we utilized zebrafish (*Danio rerio*) as the model. The structure and function of the mammalian HPA axis and the teleostean HPI axis are highly conserved (Wendelaar Bonga, 1997; Lohr and Hammerschmidt, 2011). In mammals, the CRH neurons that are principally involved in HPA-axis activation are in the hypothalamic paraventricular nucleus (PVN). In teleosts (ray-finned fish), the neuroendocrine preoptic area (NPO) is ontogenically equivalent to the PVN, and CRH neurons within the NPO perform similar roles as their mammalian counterparts (Herget and Ryu, 2015). CRH neurons in other hypothalamic regions in the zebrafish (e.g., intermediate hypothalamus) may also regulate the HPI axis (Wagle et al., 2022). A unique advantage of the zebrafish system is its rapid and external development. The development of the HPI axis begins between 1 and 2 days post fertilization (dpf), and stress-induced cortisol signaling and behaviors can be observed at 4–5 dpf (Alsop and Vijayan, 2008; Alderman and Bernier, 2009; Bai et al., 2016). The rapid development and translucency of zebrafish allow direct microscopic observation of CRH neuron development in intact, developing animals.

In this study, we investigated the roles of a conserved neuronal signaling molecule—*Down syndrome cell adhesion molecule-like 1* (zebrafish gene: *dscaml1;* mouse gene: *Dscaml1;* Human gene: *DSCAML1*; Protein: DSCAML1). DSCAML1 is one of two DSCAM family members in vertebrates, the other being DSCAM (Garrett et al., 2012). Unlike invertebrate DSCAMs, vertebrate DSCAMs are not significantly alternatively spliced (Sanes and Zipursky, 2020). In the mammalian retina, DSCAML1 prevents excessive aggregation between cells and promotes developmental cell death (Fuerst et al., 2009; Garrett et al., 2016). DSCAML1 also acts to refine synaptic specificity and synapse number (Yamagata and Sanes, 2008; Sachse et al., 2019). In humans, rare variants in *DSCAML1* are associated with several neurodevelopmental disorders, including autism spectrum disorder, cortical abnormality, and epilepsy (Iossifov et al., 2014; Karaca et al., 2015; Hayase et al., 2020; Ogata et al., 2021). Genetic and epigenetic studies also implicate *DSCAML1* in the stress response to violent experiences (Caramillo et al., 2015; Saadatmand et al., 2021). However, the relationship between *DSCAML1* and the stress axis remains unknown.

Using zebrafish, we previously explored how DSCAML1 affects neural pathways and systemic functions (Ma et al., 2020a; Ma et al., 2020b). We found that *dscaml1* deficiency resulted in various physiological and behavioral deficits, including darker pigmentation, slower light adaptation, and slower eye movements (saccades) (Ma et al., 2020b). Interestingly, darker pigmentation and slower light adaptation can also be caused by abnormal glucocorticoid receptor signaling, as seen in the zebrafish *glucocorticoid receptor* (*gr*) mutants, suggesting that the stress axis may be dysfunctional in *dscaml1* mutants (Griffiths et al., 2012; Muto et al., 2013).

Here, we report that *dscaml1* deficiency in zebrafish perturbs hypothalamic CRH neuron development and impairs the normal function of the HPI axis. These findings show that DSCAML1 is necessary for stress axis development and raise the possibility that stress dysfunction contributes to human *DSCAML1*-linked disorders.

Results

dscaml1 deficiency results in overexpression of neuroendocrine factors

To gain an unbiased view of the molecular changes resulting from *dscaml1* deficiency, we compared the transcriptomic profiles between *dscaml1* homozygous mutant (*dscaml1*−/−) and control (wild type) siblings using RNA sequencing (RNA-seq). cDNA from whole 3.5–4 days post-fertilization (dpf) *dscaml1*−/− and control larvae were sequenced using an Illumina next-generation sequencer. Using a threshold of at least two-fold change and an adjusted *p*-value of less than 0.01, we identified 25 upregulated and 79 downregulated genes (Figure 1A, Supplementary Datasheet S1).

Among the 25 upregulated genes in the *dscaml1*−/− animals, seven were secreted neuropeptides/hormones expressed in the hypothalamus or pituitary: *corticotropin-releasing hormone b (crhb)*, *parathyroid hormone 2* (*pth2*), *somatolactin beta (smtlb), cocaine- and amphetamine-regulated transcript 3 (cart3), proopiomelanocortin a (pomca), arginine vasopressin (avp),* and *spexin hormone (spx).* Among them, three (*crhb, avp, pomca*) are core regulators of the HPI axis (Alsop and Vijayan, 2009; Lohr and Hammerschmidt, 2011). *crhb* encodes the zebrafish CRH; *avp* encodes the neuropeptide AVP that controls osmolarity, blood pressure, and synergizes with CRH to promote cortisol release;

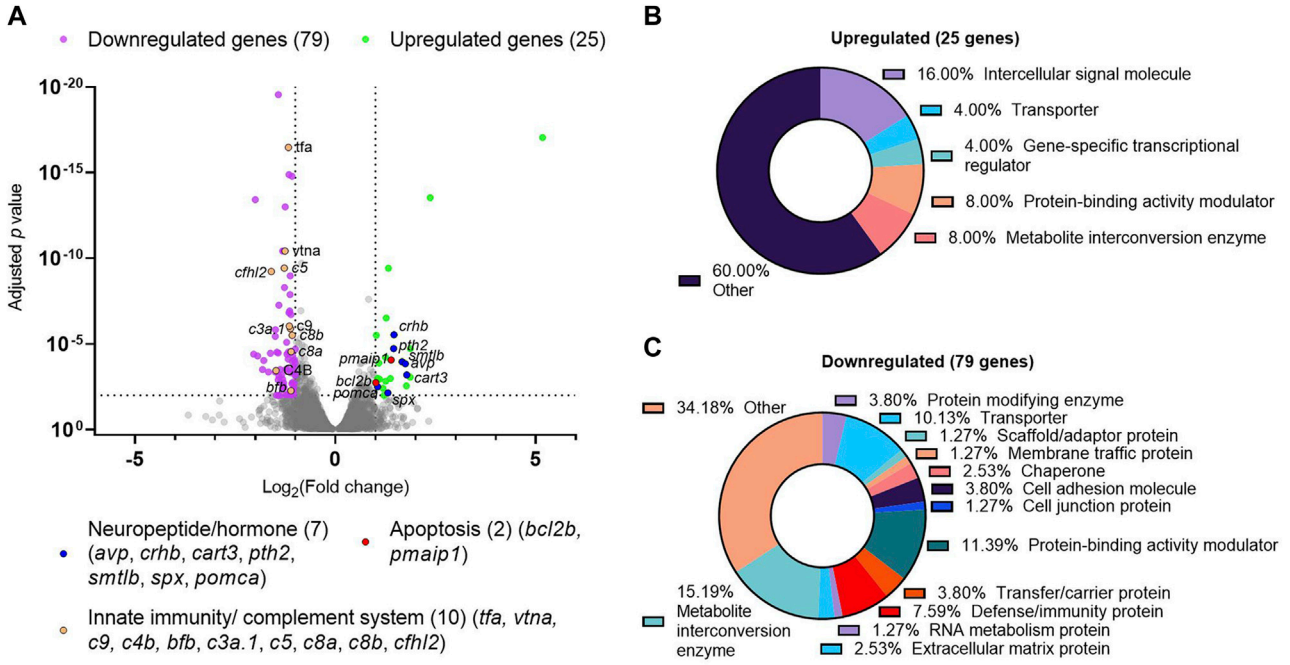

D

GO molecular function (complete)	Number of genes	Over (+) /Under(-)	*p* value
hormone activity (GO:0005179)	8	+	4.40E-05
signaling receptor activator activity (GO:0030546)	10	+	6.19E-06
signaling receptor regulator activity (GO:0030545)	10	+	6.19E-06
receptor ligand activity (GO:0048018)	10	+	6.19E-06

FIGURE 1
Differential gene expression analysis of *dscaml1* deficient zebrafish. **(A)** Volcano plot of relative gene expression in *dscaml1−/−* versus control animals. Each dot represents an individual gene, with colored dots representing gene groups as indicated on the graph. The dotted lines show the significance level (adjusted $p < 0.01$) and fold change (increase or decrease by two-fold or more) thresholds **(B, C)** Protein class categorization analysis for upregulated **(B)** and downregulated **(C)** genes. **(D)** Table of significantly enriched ($p < 0.05$) GO terms for molecular function.

pomca encodes the adrenocorticotropic hormone (ACTH), the primary pituitary hormone that triggers glucocorticoid release. Additionally, two genes involved in apoptosis are upregulated: *BCL2 apoptosis regulator b* (*bcl2b*) and *phorbol-12-myristate-13-acetate-induced protein 1* (*pmaip1/noxa*). Protein class categorization analysis with PANTHER revealed "intercellular signal molecule" as the largest class (4 genes, 16%) (Figure 1B) (Mi et al., 2021).

The 79 genes downregulated in the *dscaml1−/−* animals are more diverse in function compared to the upregulated genes. Protein class categorization analysis with PANTHER identified the largest protein classes as metabolite interconversion enzymes (12 genes, 15.19%), protein-binding activity modulators (9 genes, 11.39%), transporters (8 genes, 10.13%), and defense/immunity protein (6 genes, 7.59%) (Figure 1C). We noted that 30 of the 79 (38%) downregulated genes are highly expressed in the liver, and 10 of these genes are involved in innate immunity and the complement cascade (Figure 1A, Supplementary Datasheet S2). These results suggest that liver function and innate immunity may be suppressed in the *dscaml1* mutants.

To identify the signaling pathways affected by *dscaml1* deficiency, we analyzed all differentially expressed genes ($p < 0.01$, 210 mapped genes) using the statistical enrichment test (PANTHER Classification System, version 17.0) (Mi et al., 2021). All significantly enriched (FDR < 0.05) Gene Ontogeny (GO) terms for molecular function relate to the parent GO term *hormone activity* (Figure 1D). The PANTHER pathway analysis also identified another significant stress-modulating neuropeptide, *adenylate cyclase activating polypeptide 1b* (*adcyap1b*, also known as *PACAP*) that is significantly upregulated (0.66 fold change, adjusted $p < 0.0001$) (Stroth et al., 2011).

Together, our transcriptomic analyses indicate that *dscaml1* deficiency results in the upregulation of neuropeptide/hormonal signaling and the downregulation of liver and innate immune function. Suppression of liver and immune function is a hallmark of stress axis activation, which is consistent with the overexpression of the principal neuropeptides involved in the stress axis (*crhb, avp, pomca,* and *adcyap1b*).

10.3389/fcell.2023.1113675

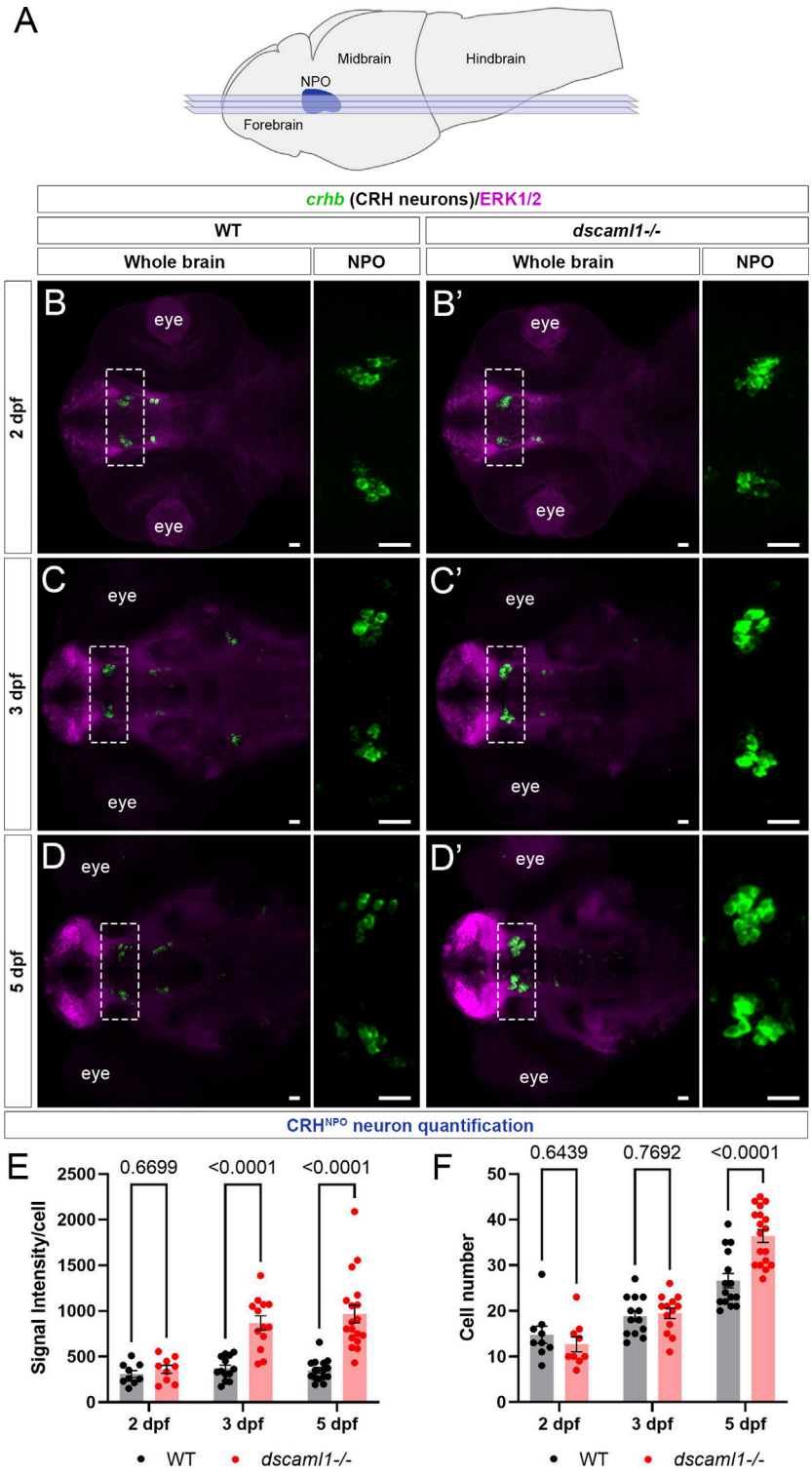

FIGURE 2
dscaml1 deficiency alters the development of CRH^{NPO} neurons. **(A)** Illustration of the larval zebrafish brain (lateral view) with rostral to the left. The NPO is highlighted in blue. Imaging planes used for CRH^{NPO} neuron analysis are shown (light blue planes) **(B-D')** Developmental trajectory of CRH^{NPO} neurons, labeled by *crhb* FISH (green) and co-stained with anti-ERK1/2 (magenta). At each developmental stage, a representative confocal sub-stack containing the NPO is shown, with the NPO (boxed region) enlarged and shown in the right panel without the ERK1/2 co-stain. Wild-type (WT) animals are shown in panels B, C, and **(D)** *dscaml1–/–* animals are shown in panels B', C', and D' **(E–F)** Quantification of the signal intensity per cell **(E)** and cell number **(F)**. Multiple-comparison corrected *p* values are as shown. WT: n = 9 (2 dpf), 13 (3 dpf), 15 (5 dpf). *dscaml1–/–*: n = 9 (2 dpf), 13 (3 dpf), 18 (5 dpf). Scale bars are 20 μm. Mean, standard error, and corrected *p* values are shown.

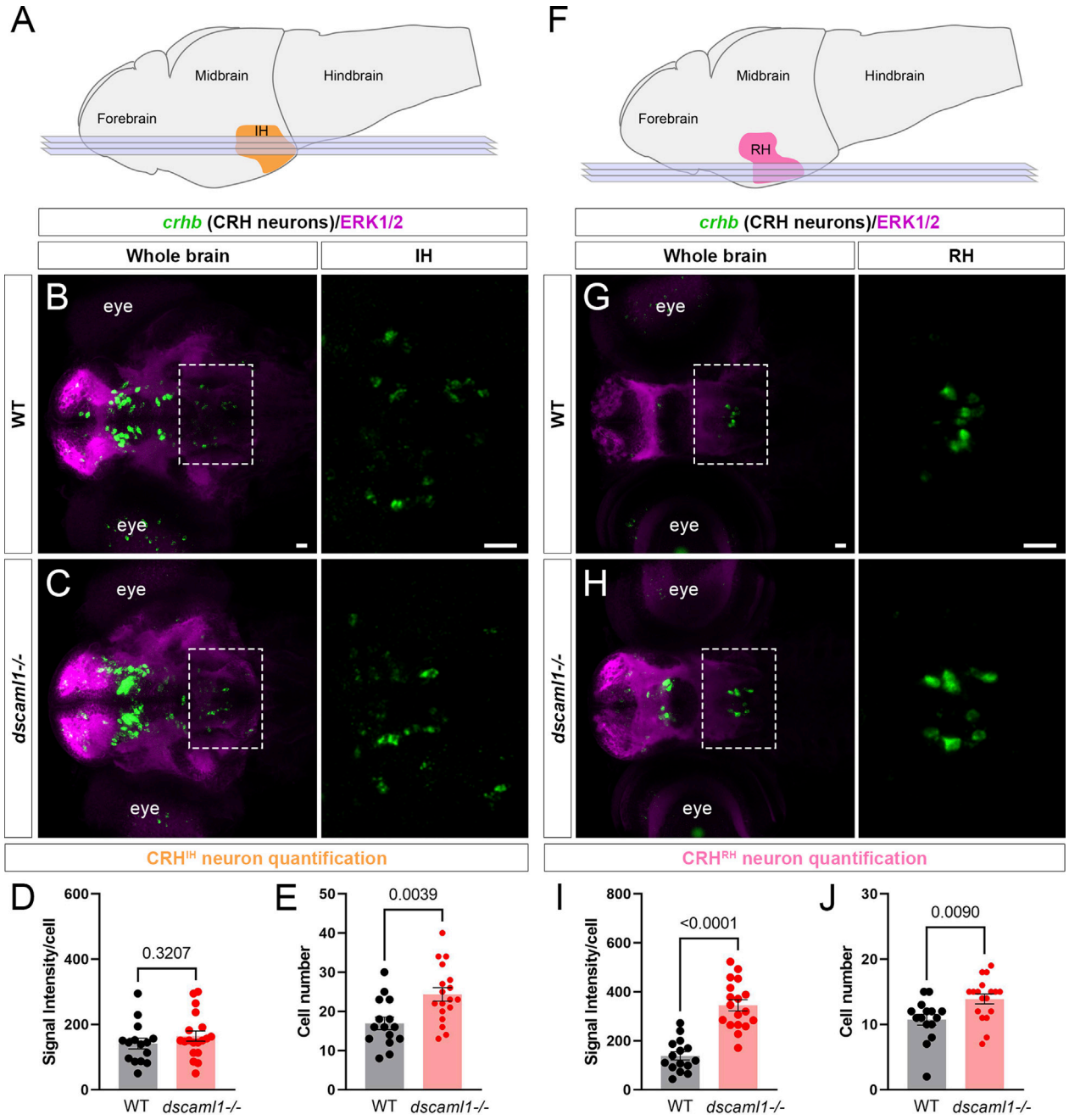

FIGURE 3
dscaml1 deficiency alters the development of CRH neurons in the intermediate and rostral hypothalamus. **(A)** Illustration of the larval brain, with the IH highlighted in orange. Imaging planes used for CRH^{IH} neuron analysis are shown (light blue planes). **(B, C)** Labeling of CRH^{IH} neurons by *crhb* FISH (green) and co-stained with anti-ERK1/2 (magenta). Representative confocal sub-stacks containing the IH are shown, with the IH (boxed region) enlarged and shown in the right panel without the ERK1/2 co-stain. WT brain is shown in panel B and *dscaml1–/–* brain is shown in panel **C**. **(D–E)** Quantification of the signal intensity per cell **(D)** and cell number **(E)**. **(F)** Illustration of the larval brain, with the RH highlighted in pink. Imaging planes used for CRH^{RH} neuron analysis are shown (light blue planes). **(G–H)** Labeling of CRH^{RH} neurons by *crhb* FISH (green) and co-stained with anti-ERK1/2 (magenta). Representative confocal sub-stacks containing the RH are shown, with the RH (boxed region) enlarged and shown in the right panel without the ERK1/2 co-stain. WT brain is shown in panel G and *dscaml1–/–* brain is shown in panel **H**. **(I–J)** Quantification of the signal intensity per cell **(I)** and cell number **(J)**. WT: n = 15. *dscaml1–/–*: n = 18. Scale bars are 20 μm. Mean, standard error, and *p* values are shown.

dscaml1 deficiency alters the development of CRH neurons in the NPO

To further investigate whether the stress axis is perturbed in *dscaml1* mutants, we first examined the development of CRH neurons in the NPO (CRH^{NPO} neurons) (Figure 2A), which are localized in the dorsal preoptic area and characterized by their expression of *crhb* (Herget et al., 2014; Vom Berg-Maurer et al., 2016). We focused on three developmental stages (2, 3, and 5 dpf) that span the period between the first appearance of *crhb* + neurons

in the NPO (2 dpf) and the onset of stress axis responsivity (4–5 dpf) (Chandrasekar et al., 2007; Alderman and Bernier, 2009; Clark et al., 2011). Sibling controls were used for all comparisons.

Using fluorescent *in situ* hybridization (FISH), we found that *crhb* expression pattern was initially similar between *dscaml1*−/− and wild-type (WT) animals at 2 dpf (Figure 2B, B'). At 3 dpf, we began to see higher *crhb* expression in the NPO of *dscaml1*−/− animals (Figure 2C, C'), and *crhb* expression in the NPO remains higher in *dscaml1*−/− animals at 5 dpf (Figure 2D, D"). Quantification of *crhb* FISH signal intensity among CRH^{NPO} neurons showed that *crhb* expression is higher in *dscaml1*−/− animals, compared to WT animals (Figure 2E). There was a significant difference in signal intensity per cell by developmental stage and genotype, and a significant interaction between stage and genotype (two-way ANOVA, Supplementary Table SI). Pair-wise comparisons with Holm-Sidak correction found a significant increase at 3 and 5 dpf but not at 2 dpf (Figure 2E).

In addition to changes in *crhb* expression levels, *dscaml1* deficiency also increased the number of *crhb*-expressing CRH^{NPO} neurons. In WT animals, the number of CRH^{NPO} neurons increased over time, from 14.78 cells (2 dpf) to 18.85 cells (3 dpf) to 26.60 cells (5 dpf) per animal (Figures 2B–D, F). In *dscaml1*−/− animals, the number of CRH^{NPO} neurons increased at a higher rate, from 12.67 cells (2 dpf) to 19.46 cells (3 dpf) to 36.39 cells (5 dpf) per animal (Figure 2B', C', D', F). There was a significant difference in cell number by developmental stage and genotype, and there was a significant interaction between stage and genotype (Two-way ANOVA, Supplementary Table SI). Pair-wise comparisons with Holm-Sidak correction found a significant increase in cell number between *dscaml1*−/− and WT animals at 5 dpf but not at 2 and 3 dpf (Figure 2F, adjusted *p* values as shown).

Overall, we found significant increases in *crhb* expression and cell number in CRH^{NPO} neurons in *dscaml1*−/− mutants as compared to WT. These phenotypes were not due to the visual deficits in *dscaml1*−/− animals (Ma et al., 2020b), as similar phenotypes were observed in animals raised in the dark (Supplementary Figure S1). Together, these findings show that *dscaml1* is essential for the normal developmental trajectory of CRH^{NPO} neurons.

dscaml1 deficiency impairs CRH neuron development in the intermediate and rostral hypothalamus

To test whether other hypothalamic CRH neurons are affected similarly to CRH^{NPO} neurons, we examined two additional *crhb*-expressing hypothalamic regions. In zebrafish, the intermediate hypothalamus (IH) CRH neurons (CRH^{IH} neurons) regulate stress response and the perception of the emotional valence of light (Figure 3A) (Wagle et al., 2022). In the IH at 5 dpf, we did not observe any significant difference in *crhb* expression levels (FISH intensity) between *dscaml1*−/− and WT animals (Figures 3B–D). However, the number of CRH^{IH} neurons was significantly higher in *dscaml1*−/− animals (unpaired *t*-test, Figure 3E).

In addition to the IH, we have found consistent *crhb* expression in the rostral hypothalamus (RH) (Figure 3F). The roles of CRH neurons in the RH (CRH^{RH} neurons) are still unknown, but they may contribute to the rostral hypothalamus-optic tectum pathway (Heap et al., 2017). In the RH at 5 dpf, both the *crhb* expression levels and the CRH^{RH} cell number were higher in *dscaml1*−/− animals compared to WT (unpaired *t*-test, Figures 3G–J). Thus, *dscaml1* is required broadly to regulate CRH neuron cell number in the developing hypothalamus, but *dscaml1* deficiency only affects *crhb* expression in the RH and NPO.

Programmed cell death in the hypothalamus is reduced in *dscaml1* mutants

DSCAM family proteins are known to reduce neuronal cell number by promoting PCD in the mammalian retina (Fuerst et al., 2012; Garrett et al., 2016). Additionally, our transcriptomic analysis showed that *dscaml1* mutants express higher levels of apoptosis-regulating genes, *bcl2b* and *pmaip1* (Figure 1A). Therefore, we hypothesized that *dscaml1* deficiency might impair PCD in the developing hypothalamus.

To test this, we used an anti-activated caspase 3 (AC3) antibody to label apoptotic cells (Pyati et al., 2011). In wild-type animals, we saw widespread apoptosis in the nervous system, peaking at 3 dpf (Figure 4A–A"), consistent with previous findings using TUNEL (Cole and Ross, 2001). We found a decrease in AC3-positive cells in *dscaml1*−/− animals at 3 and 5 dpf, compared to wild-type sibling controls (Figure 4B–B"). To quantify the amount of cell death in specific hypothalamic regions, we used the Map-map calculation and the Z-Brain anatomical atlas (Randlett et al., 2015). In this method, individual confocal image stacks are registered to the Z-Brain reference brain; registered stacks are then grouped by genotype for voxel-wise comparisons using the Mann-Whitney *U*-statistic (WT n = 14; *dscaml1*−/− n = 21). The voxels with significant Z-scores, either higher in WT (WT over *dscaml1*) or higher in *dscaml1*−/− (*dscaml1* over WT), were mapped to regions of interest (ROIs) and the mean voxel values in each ROI were calculated and displayed using a green-magenta color scale (green: higher in WT; magenta: higher in *dscaml1*−/−) (Figure 4C).

Overall, AC3 signal is higher in WT throughout the brain, compared to *dscaml1*−/− (*i.e.*, many green regions and very few magenta ROIs). Out of 293 ROIs annotated in Z-Brain, 178 had voxels with significant WT over *dscaml1* signal (mean signal = 1,384.90) (WT over *dscaml1* sheet, Supplementary Datasheet S3). In contrast, only 65 ROIs had voxels with significant *dscaml1* over WT signal (mean signal = 84.23) (*dscaml1* over WT sheet, Supplementary Datasheet S3).

In the ROIs corresponding to the hypothalamic *crhb* expressing areas, the NPO (Z-Brain ROI: Diencephalon—Otpb Cluster 2) (WT over *dscaml1* signal = 5,688.06; *dscaml1* over WT signal = 0), IH (Diencephalon - Intermediate Hypothalamus) (WT over *dscaml1* signal = 673.56; *dscaml1* over WT signal = 36.40), and RH (Diencephalon - Rostral Hypothalamus) (WT over *dscaml1* signal = 916.95; *dscaml1* over WT signal = 0.70) all had higher AC3 signal in WT, compared to *dscaml1*−/− (Figures 4D–F). Together, these results suggest that reduced PCD in *dscaml1*−/− animals may contribute to the higher number of CRH neurons in the hypothalamus.

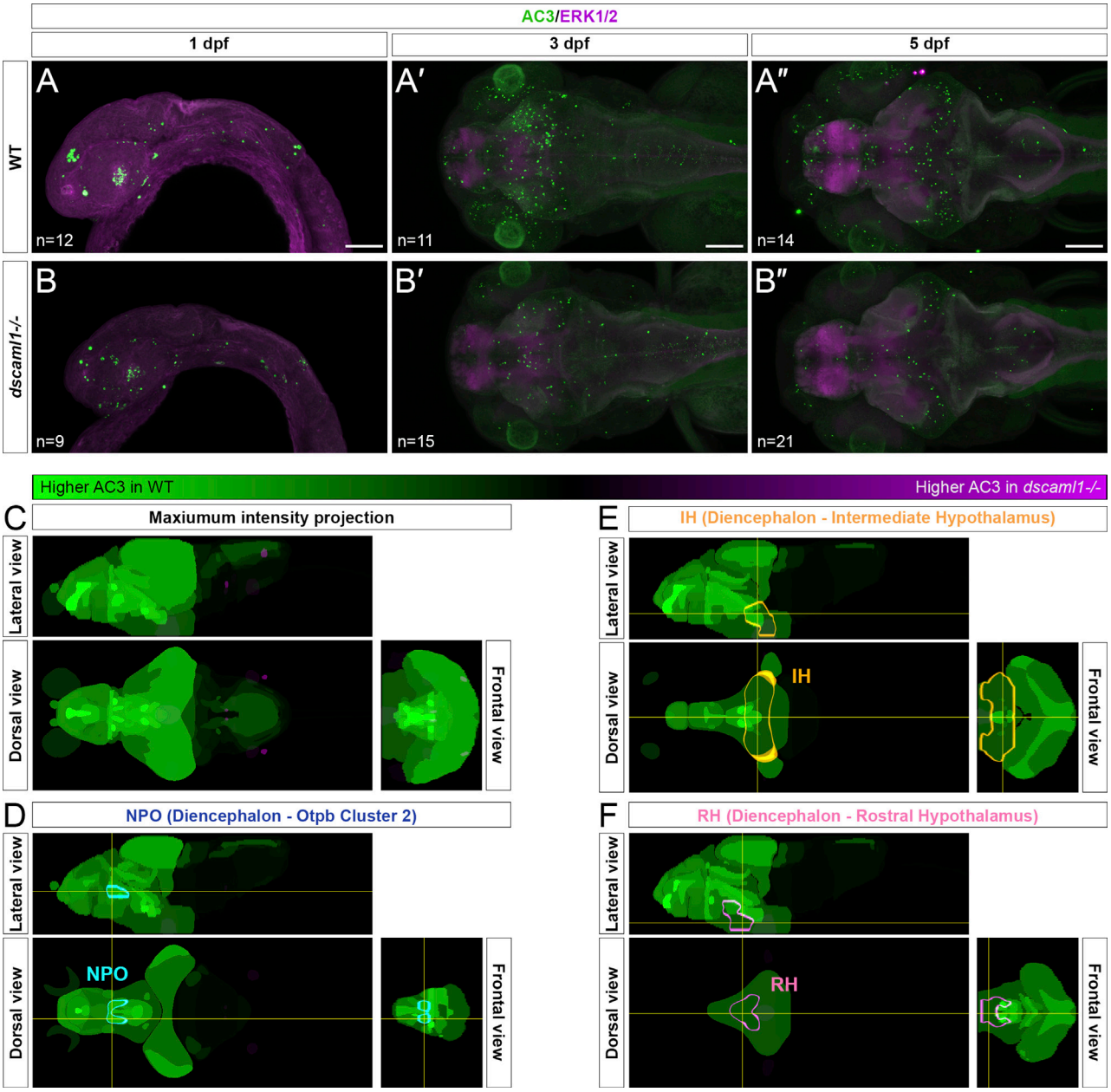

FIGURE 4
Programmed cell death in the brain is reduced in *dscaml1* mutants. **(A–B″)** Immunolabeling with anti-AC3 (green) and counterstained with anti-ERK1/2 (magenta). 1 dpf embryos are shown laterally, and 3 and 5 dpf larvae dorsally. Wild-type (WT) animals are shown in panels **A–A″** and *dscaml1–/–* animals are shown in panels **B–B″**. **(C)** 5 dpf Z-Brain mapping of brain regions, showing regions with higher AC3 labeling in WT (green) or *dscaml1–/–* (magenta). Orthogonal maximum intensity projections are shown. **(D)** Z-Brain mapping in the NPO. Z-Brain ROI name is indicated in the parenthesis. Orthogonal sections are shown. **(E)** Z-Brain mapping in the IH. Z-Brain ROI name is indicated in the parenthesis. Orthogonal sections are shown. **(F)** Z-Brain mapping in the RH. Z-Brain ROI name is indicated in the parenthesis. Orthogonal sections are shown. Anterior is to the left for all images. Scale bars are 100 µm.

dscaml1 is essential for normal CRH^{NPO} neuron cell death

To further determine whether *dscaml1* affects the survival of hypothalamic CRH neurons, we tracked the fate of individual CRH^{NPO} neurons using *in vivo* time-lapse imaging at 3 to 5 dpf, when cell number begins to diverge between *dscaml1–/–* and WT animals. To visualize CRH^{NPO} neurons in live zebrafish, we generated a *crhb* knock-in fluorescent reporter line using CRISPR-mediated genomic insertion (Figure 5A) (Kimura et al., 2014). A Cre-switchable *hsp-LoxP-RFP-LoxP-GFP* cassette was inserted 35 base pairs upstream of the first exon of *crhb* so that the expression of RFP (default) or GFP (with Cre-mediate recombination) would mark the endogenous *crhb*-expressing cells (Figure 5B). The resulting transgenic line, *crhb:LoxP-RFP-LoxP-GFP* (*crhb:LRLG*), has RFP and GFP

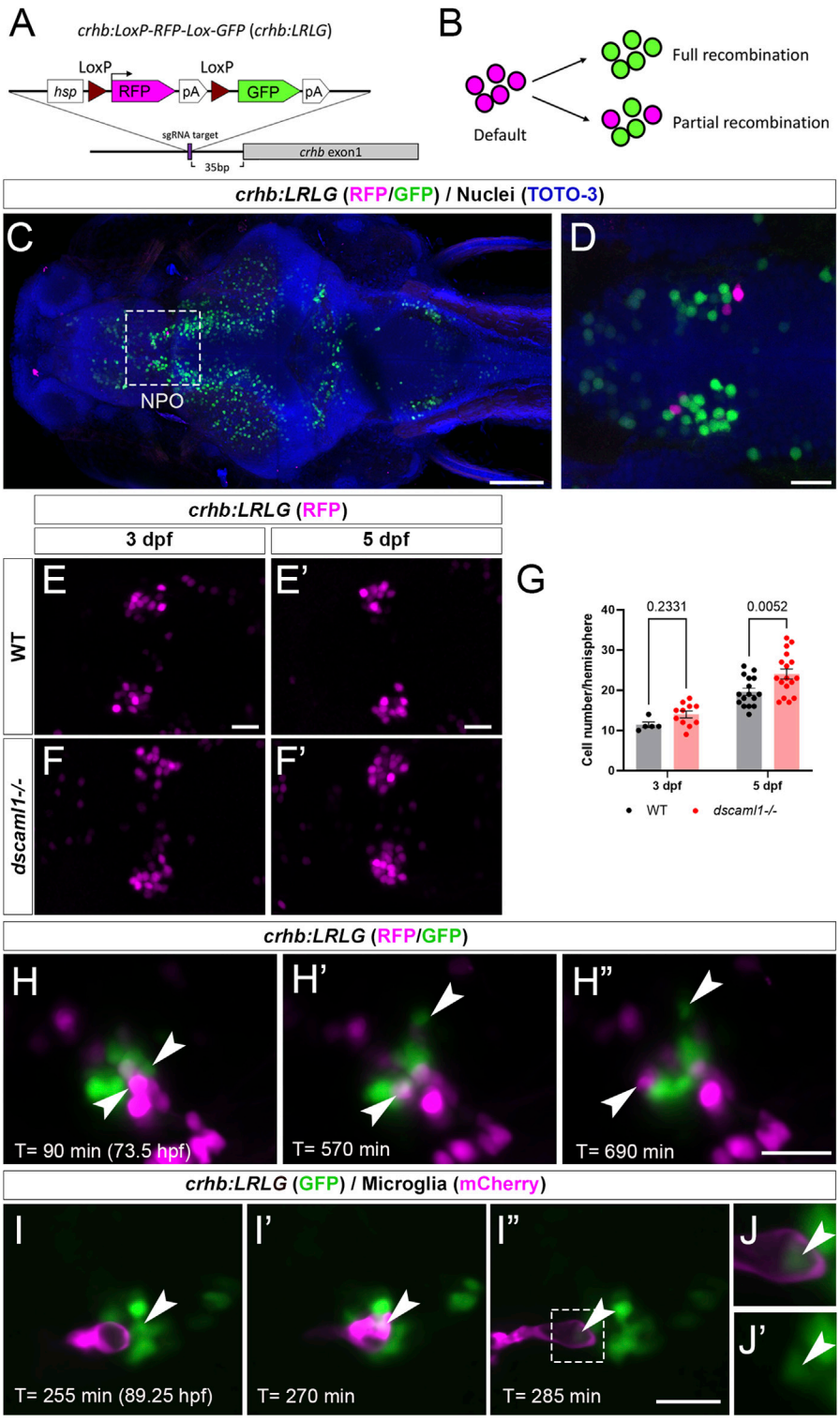

FIGURE 5
Fluorescent labeling and live imaging of CRH^{NPO} neurons. **(A)** Schematic of CRISPR -mediated knock-in of the *hsp-Lox-RFP-Lox-GFP* cassette at the sgRNA target site, located 35 bp upstream of exon 1 of *crhb*. The orientation and junctional structure of insertion have not been determined. **(B)** Schematic of *crhb:LRLG* expression. Each circle represents a fluorescent cell. Without Cre (default), RFP is expressed in all cells. With full recombination, all cells express GFP. Partial recombination results in mosaic RFP and GFP labeling. **(C)** Dorsal view of a fixed 5 dpf *crhb:LRLG* larvae with partial recombination stained with anti-RFP (magenta) and anti-GFP (green). The boxed area marks the NPO. **(D)** Higher magnification image of the NPO. Both RFP and GFP-positive neurons can be seen. **(E-F')** Images of anti-RFP stained *crh:LRLG* animals without recombination. Representative WT (E-E') and *dscaml1–/–* **(F-F')** NPO neurons are shown. **(G)** Quantification of RFP-positive cells at 3 and 5 dpf. WT: n = 5 (3 dpf), 16 (5 dpf). *dscaml1–/–*: n = 11 (3 dpf), 17 (5 dpf). Mean, standard error, and corrected *p* values are shown. **(H–H")** Live *crhb:LRLG* larvae with partial recombination were imaged from 72 to 84 hpf. Three time points are shown here. Two cells (arrowheads, one green and one magenta) move away over time. **(I–I")** Live *crhb:LRLG;mpeg1:Gal4;UAS:NTR-mCherry* larvae with CRH neurons labeled with GFP (green) and
(*Continued*)

FIGURE 5 (Continued)
microglia labeled with mCherry (magenta). In this image series, one CRH neuron (arrowhead) is engulfed **(I')** and then removed **(I")** by a microglial cell. Images are confocal optical sections. **(J, J')** Panels showing enlarged views of the boxed area in **(I")**, with **(J)** or without **(J')** the mCherry channel. The remnant of the CRH neuron can still be seen inside the microglia (arrowheads). Scale bars are 100 μm (panel C) or 20 μm (all other images).

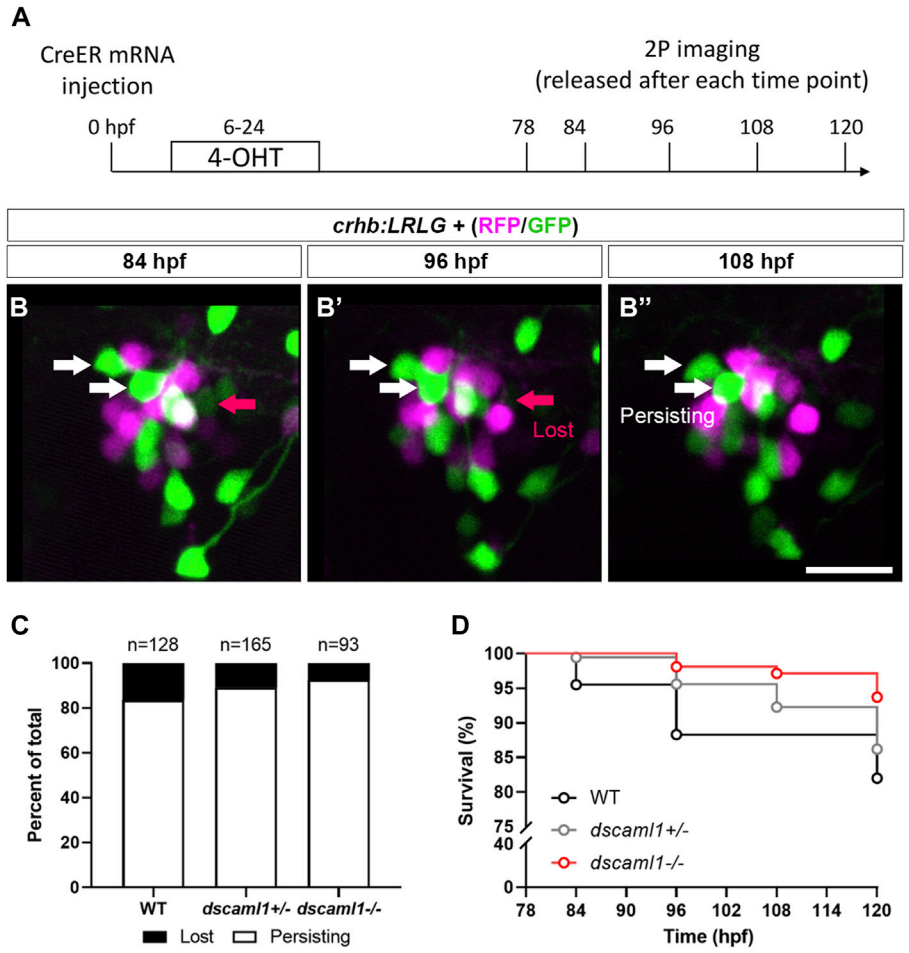

FIGURE 6
Live tracking of CRH^{NPO} neuron cell fate. **(A)** Timeline of time-lapse two-photon (2P) imaging experiment. Partial recombination of *crhb:LRLG* was induced by 4-OHT at 6–24 hpf, and imaging was performed at 78, 84, 96, 108, and 120 hpf. Animals were briefly anesthetized during imaging and allowed to recover in between imaging sessions. **(B–B")** Tracking of individual CRH^{NPO} neurons. Three example time frames are shown. Individual fluorescent cells can be tracked over time and are divided into two categories: persisting (white arrows) or lost (pink arrow). The scale bar is 20 μm. **(C)** Quantification of the percentage of persisting versus lost CRH^{NPO} neurons. Sample size (cell number) as indicated for each genotype. **(D)** Survival curve of individual CRH^{NPO} neurons in each genotypic group.

expression pattern that matches the endogenous *crhb* transcript expression patterns reported by others (Figures 5C, D) (Shainer et al., 2022). To validate the fidelity of fluorescent reporter expression, we examined whether *crhb:LRLG*-labeled cells in the NPO express CRH protein. In animals not exposed to Cre (default RFP expression), we found that most RFP+ neurons are CRH immunopositive (84.71% ± 2.19%, Supplementary Figure S2A–B). Together, these results indicate that the *crhb:LRLG* line reliably labels CRH^{NPO} neurons.

In *crhb:LRLG* animals, *dscaml1* deficiency increased the number of RFP-labeled CRH^{NPO} neurons (Figure 5E–F'). There were significant differences by developmental stage and genotype, with no significant interaction (two-way ANOVA, Supplementary Table SI). There was a significantly higher number of RFP-positive neurons in the *dscaml1* mutants at 5 dpf but not 3 dpf (Figure 5G, multiple comparison test with Holm-Sidak correction). This result corroborates our *crhb* FISH results that show increased CRH^{NPO} neuron number in *dscaml1* mutants (Figure 2F).

Using the *crhb:LRLG* line, we first performed time-lapse imaging in anesthetized animals. We induced partial Cre-mediated recombination by injecting *CreER* mRNA into *crhb:LRLG* animals at the 1-cell stage and adding 4-hydroxytamoxifen (4-OHT) to activate CreER at 6–24 hpf (Figure 5B). At 3–4 dpf,

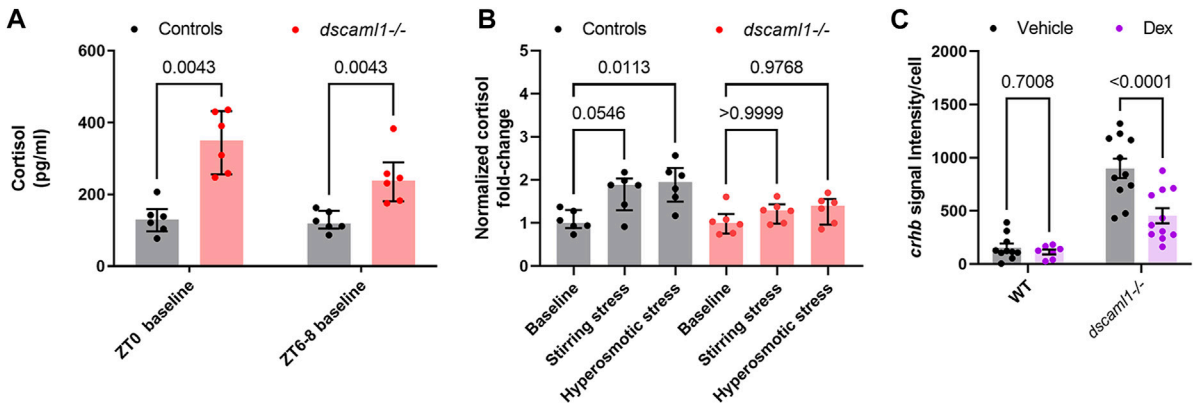

FIGURE 7
Cortisol levels and response to exogenous glucocorticoids. **(A–B)** Cortisol profile for 5 dpf larvae. For each sample (dot), cortisol was extracted from a pool of 30 animals. n = 6 for all groups. Median, interquartile range, and corrected *p* values are shown. **(A)** Baseline cortisol in control (black) and *dscaml1*−/− (red) animals. **(B)** Baseline-normalized cortisol fold change in control (black) and *dscaml1*−/− (red) animals. **(C)** Quantification of *crhb* signal intensity per cell in CRH^{NPO} neurons. Vehicle: n = 10 (WT), 11 (*dscaml1*−/−). Dex: n = 7 (WT), 11 (*dscaml1*−/−). Mean, standard error, and corrected *p* values are shown.

intermingled GFP+ and RFP+ cells can be seen in the NPO by confocal imaging (Figure 5H–H" and Supplementary Video S1). Over time, some labeled cells moved away from the CRH^{NPO} neuron cluster. These cells were likely dying cells being carried away by microglia, as seen in previous zebrafish studies (Mazaheri et al., 2014). To confirm this, we induced GFP expression (by injecting codon-optimized *Cre* mRNA) (Horstick et al., 2015) in all *crhb:LRLG*-labeled cells and labeled microglia with the *mpeg1:mCherry* transgene (Figure 5I–I" and Supplementary Video S2) (Espenschied et al., 2019). Indeed, mCherry+ microglia migrated toward the GFP+ cell cluster, engulfed GFP+ CRH^{NPO} neurons, and carried the engulfed cells away. The remnant of the engulfed cell can be seen inside a large vacuole within the microglia (Figure 5J, J'). This type of engulfment events was seen in three out of five animals between 3.5-4 dpf. These results suggest that CRH^{NPO} neurons undergo PCD and that dying cells are rapidly removed by microglia.

Next, to track the fate of individual CRH^{NPO} neurons, we performed two-photon imaging from 3 to 5 dpf on *crhb:LRLG* animals with partial Cre-mediated recombination (Figure 6A). To minimize the potential effects of stress on PCD (Irles et al., 2014), we anesthetized and immobilized the animals during imaging. In between imaging sessions, each animal is allowed to recover in individual wells of 12-well plates, under normal light-dark cycles. Cells that are present at the first time point (78 hpf) were tracked at four subsequent time points (84, 96, 108, and 120 hpf) and categorized as either persisting (present at the last time point) or lost (lost at any of the following time points) (Figure 6B–B"). Overall, we observe a trend of reduced cell loss in the *dscaml1*+/− and *dscaml1*−/− animals (Chi-square test for trend, $p = 0.0398$) (Figure 6C, total number of tracked cells as indicated). In WT animals, 16.41% of cells are lost, versus 10.91% and 7.53% for *dscaml1*+/− *and dscaml1*−/−, respectively.

Finally, considering the timing of cell loss, we plotted the survival curve of CRH^{NPO} neurons for each genotype. Again, there was a significant difference in the trends of cell loss (Logrank test for trend, $p = 0.0098$), with the *dscaml1*−/− animals consistently showing a higher survival rate (Figure 6D). Together, these results show that *dscaml1* deficiency reduces PCD of CRH^{NPO} neurons.

Stress axis function is perturbed in *dscaml1* mutant animals

Given the developmental perturbation of hypothalamic CRH neurons as well as the global changes in gene expression related to stress axis activation, we next determined whether the hormonal output of the stress axis—cortisol—is altered. Cortisol levels were measured using an enzyme-linked immunosorbent assay (ELISA) on homogenates made from pools of 5 dpf animals (30 animals per sample, 6 samples per condition). All animals were raised under standardized conditions, at the same density, and with a normal circadian cycle (14 h day/10 h night) (Yeh et al., 2013). Under this circadian cycle, *dscaml1* mutant animals exhibit similar diurnal locomotor rhythms as wild-type animals (Ma et al., 2020b).

Baseline and stressed conditions were tested to evaluate potential alterations of cortisol in control (WT and *dscaml1*+/−) and *dscaml1*−/− siblings at 5 dpf. To measure baseline cortisol, we collected unperturbed animals within 30 min after light onset (zeitgeber time 0, ZT0) and in the afternoon (ZT6-8). To measure stress-induced cortisol, animals were exposed to either stirring stress (swirling water, 5 min) (Castillo-Ramirez et al., 2019) or hyperosmotic stress (250 mM NaCl, 20 min) at ZT6-8 (Yeh et al., 2013). These acute stressors are well-characterized and are comparable to the water current and salinity changes experienced by zebrafish larvae in their natural habitat (Clark et al., 2011).

At baseline, *dscaml1*−/− animals had significantly higher cortisol levels than control animals (Multiple Mann-Whitney test with Holm-Sidak correction. Adjusted *p* values shown in Figure 7A). At ZT0, the *dscaml1* mutant baseline cortisol levels were 2.7-fold higher than that of

controls (median 350.06 pg/mL versus 129.80 pg/mL). The difference in cortisol was less pronounced at ZT6-8, but *dscaml1* mutants still had 2-fold higher cortisol levels than controls at baseline (median 238.51 pg/mL versus 118.52 pg/mL).

After acute exposure to stressors, we found that *dscaml1* mutant animals exhibited attenuated cortisol induction. We assessed the extent of stress-induced cortisol production by normalizing cortisol levels to the baseline cortisol of the same genotype at the same circadian time (ZT6-8). In the control group, stirring stress and hyperosmotic stress produced 1.88 and 1.95-fold increases in cortisol over the control baseline, respectively (grey bars, Figure 7B) (non-normalized cortisol data are shown in Supplementary Figure S3). The response to hyperosmotic stress was more robust (p = 0.0113, Multiple Mann-Whitney tests with Holm-Sidak correction) than that generated by stirring stress (p = 0.0546). In the *dscaml1*−/− group, stirring stress and hyperosmotic stress only produced 1.29 and 1.4-fold increases in cortisol over the *dscaml1*−/− baseline, respectively (red bars, Figure 7B). These increases were not statistically significant (p > 0.9999 for stirring stress, p = 0.9768 for hyperosmotic stress).

Together, these results show that *dscaml1* deficiency elevates baseline cortisol levels and impair responses to acute stressors. These findings indicate that *dscaml1* is critical for establishing the normal function of the stress axis.

dscaml1 mutants are responsive to glucocorticoids

Some aspects of the stress axis-related phenotypes in *dscaml1* mutants resemble the zebrafish *glucocorticoid receptor (gr)* mutants. In particular, both *gr* and *dscaml1* mutants exhibit elevated baseline cortisol and *crhb* (Ziv et al., 2013). This resemblance raises the possibility that the *dscaml1* mutant phenotypes may result from insufficient glucocorticoid receptor-mediated signaling. To test this, we examined whether *dscaml1* mutants can respond transcriptionally to exogenously applied glucocorticoids. We examined the expression of *crhb* in the NPO, as it is under feedback control from glucocorticoid-glucocorticoid receptor signaling (Watts, 2005). Wild-type siblings were used for controls.

A synthetic glucocorticoid receptor agonist, dexamethasone (Dex), was added to the embryo media at a final concentration of 2 μM from 4 to 5 dpf (24 h). Vehicle (0.02% ethanol) treated siblings were used for comparison. For *crhb* transcript level in CRH^{NPO} neurons, we found significant differences caused by Dex treatment and genotype, with significant interaction between the two (two-way ANOVA, Supplementary Table SI). Multiple comparison tests found that Dex significantly reduced *crhb* transcript level in *dscaml1*−/− animals but not in wild-type animals (Holm-Sidak correction, Figure 7C with p values as indicated). These results show that *dscaml1* deficiency does not result in a loss of glucocorticoid responsivity in CRH^{NPO} neurons. Instead, *dscaml1* deficiency may render animals more sensitive to the inhibitory effects of glucocorticoids.

Discussion

The present study provides evidence that *dscaml1* regulates the development of hypothalamic CRH neurons and is necessary for normal stress axis function. At the transcriptome level, *dscaml1* deficiency in zebrafish results in gene expression changes that suggest stress axis hyperactivation. At the cellular level, we find that *dscaml1*−/− hypothalamic CRH neurons have increased stress axis-associated neuropeptide (*crhb*) expression, increased cell number, and reduced cell death. Physiologically, *dscaml1* deficiency impairs normal neuroendocrine stress axis function, which is potentially caused by developmental deficits in hypothalamic CRH neurons as well as systemic changes in hormone/neuropeptide signaling. Together, these findings link DSCAML1 to the development of the stress axis and shed new light on the potential etiology of human *DSCAML1*-linked mental health conditions.

DSCAML1 is a novel intercellular signaling molecule for CRH neuron development

A major finding of this study is that DSCAML1 is necessary for the development of hypothalamic CRH neurons. To our knowledge, DSCAML1 is the first intercellular signaling molecule to be implicated in CRH neuron development. Our finding also provides the first link between DSCAML1 and hypothalamus development. We show that, similar to retinal neurons, the regulation of cell number by PCD is a DSCAML1-mediated process in hypothalamic CRH neurons (Garrett et al., 2016). Further investigations are required to determine whether other aspects of DSCAML1 function, such as the regulation of cellular spacing and synaptogenesis, are involved in CRH neuron development (Fuerst et al., 2009; Yamagata and Sanes, 2010; Sachse et al., 2019). Additionally, given that *dscaml1* is expressed broadly in the nervous system (Ma et al., 2020b), including CRH neurons and non-CRH neurons (Supplementary Figure S4), it will be important to address whether *DSCAML1* acts cell-autonomously in CRH^{NPO} neurons.

Regulation of CRH neuron cell death by DSCAML1

During development, PCD is critical for eliminating transient cell types, matching input and output cell populations, and maintaining cellular spacing (Yamaguchi and Miura, 2015; Wong and Marin, 2019). It has been hypothesized that PCD in the hypothalamus may specify neural circuit assembly and shape output activity (Simerly, 2002; Forger, 2009). Congruent with this idea, reduced hypothalamic PCD caused by early-life stress is associated with increased sensitivity to acute stressors in adulthood (Zhang et al., 2012; Irles et al., 2014).

As an intercellular signaling molecule, DSCAML1 may act to transduce extracellular cues for PCD. One potential cue is synaptic activity, which is critical for neuronal survival during development (Wong and Marin, 2019). In culture, DSCAML1 is localized to excitatory synapses (Yamagata and Sanes, 2010) and inhibits excitatory synaptogenesis when overexpressed (Sachse et al., 2019). It remains to be determined whether DSCAML1 deficiency increases excitatory synaptic transmission

and activates activity-dependent cell survival pathways in CRH neurons (Wong and Marin, 2019).

It is worth noting that CRH neuron cell death may not be the sole mechanism by which *dscaml1* affects CRH neuron number. Changes in the number or proliferative capacity of neuroprogenitor cells may contribute to the increase CRH neuron number we observed in *dscaml1* mutants. Additionally, the higher *crhb* expression induced by *dscaml1* deficiency may lead to more cells being identified as CRH neurons. Further work is needed to determine how these factors control CRH neuron number during development.

Stress axis dysfunction in DSCAML1 deficient animals

dscaml1−/− animals exhibit multiple signs of stress axis activation at baseline, including cortisol elevation and the suppression of immunity-associated genes. The elevated baseline cortisol levels likely resulted in attenuated responses to acute stressors, similar to animals under chronic cortisol administration (Barton et al., 1987; Johnson et al., 2006). A likely cause of these phenotypes is the overexpression of *crhb*. In mice, broad overexpression of CRH leads to elevated corticosterone (the stress glucocorticoid in rodents) and produces phenotypes similar to Cushing's syndrome, a human disorder caused by the overproduction of cortisol (Stenzel-Poore et al., 1992; Arnett et al., 2016).

Beyond dysfunction of hypothalamic neurons and CRH signaling, a broader neurological imbalance can also activate the stress axis. For example, seizures have been shown to activate the HPA axis, which increases the likelihood of future seizures (O'Toole et al., 2014; Hooper et al., 2018). It has been reported that *Dscaml1* mutant rats and human patients with *DSCAML1* loss-of-function variants exhibit neuronal hyperactivation and seizures (Hayase et al., 2020). It is, therefore, possible that excitation-inhibition imbalance in extra-hypothalamic regions may result in increased hypothalamic CRH neuron firing in zebrafish *dscaml1* mutants. Further studies on the cell-type-specific functions of *dscaml1* are needed to understand the precise cause of stress axis hyperactivation in *dscaml1*−/− animals.

The interplay between cortisol signaling and CRH neuron development

Facilitation and feedback are signature features of the stress axis (Dallman et al., 1992; Spencer and Deak, 2017). While CRH neurons control cortisol levels, cortisol signaling also affects the development of CRH neurons. Zebrafish *gr* mutants have phenotypes similar to that of *dscaml1*−/− animals, including slow visual-background adaptation, sluggish light onset response, elevated cortisol, and increased expression of *crhb* (Griffiths et al., 2012; Muto et al., 2013; Ziv et al., 2013). Surprisingly, rather than decreased glucocorticoid receptor signaling (as in *gr* mutants), *dscaml1*−/− animals have intact glucocorticoid receptor signaling, with dexamethasone exerting strong suppression of *crhb* expression in the NPO. Thus, despite the superficial phenotypic similarity, the underlying signaling mechanisms are distinct between *dscaml1* and *gr* mutants.

Given the known roles of DSCAML1 in regulating synapse formation (Sachse et al., 2019), the increase in *crhb* expression may be caused by the hyper-activation of upstream stress-related neural inputs. In rodents, various paradigms of chronic stress usually result in an upregulation of CRH in the PVN (Herman and Tasker, 2016). The transcriptional activation caused by stress-related synaptic activity may overcome the negative feedback mediated by glucocorticoid receptor signaling. Additional work is needed to disambiguate the relationship between cortisol disturbances and developmental deficits. A possible approach would be to normalize cortisol levels by genetically ablating interrenal cells (i.e., genetic adrenalectomy) and supplementing with constant levels of exogenous cortisol (Gutierrez-Triana et al., 2015).

Conclusion

In conclusion, this work shows that DSCAML1 is integral for developing the hypothalamic neurons that regulate the neuroendocrine stress axis. Using zebrafish as a vertebrate model for the ontogenesis of the stress axis, we found that *dscaml1* deficiency results in CRH neuron deficits and dysfunction of the stress axis. Genetic perturbations of *DSCAML1* are seen in patients suffering from a wide range of mental health disorders, including intellectual disability, autism spectrum disorder, schizophrenia, epilepsy, and stress disorder (Iossifov et al., 2014; Caramillo et al., 2015; Karaca et al., 2015; Hayase et al., 2020; Ogata et al., 2021; Saadatmand et al., 2021). Developmental deficits in the stress axis may contribute to the etiology of these disorders.

Materials and methods

Zebrafish husbandry

Zebrafish (all ages) were raised under a 14/10 light/dark cycle at 28.5°C. Embryos and larvae were raised in E3 buffer (5 mM NaCl, 0.17 mM KCl, 0.33 mM $CaCl_2$, 0.33 mM $MgSO_4$) (Nüsslein-Volhard et al., 2002). All zebrafish used in this study were in a mixed background of AB and TL wild-type strains (Zebrafish International Resource Center). Sex was not a relevant variable for the stages used in this study (0–6 dpf), as laboratory zebrafish remain sexually undifferentiated until 2 weeks of age (Maack and Segner, 2003; Wilson et al., 2014).

Transgenic and mutant zebrafish lines

The *dscaml1*^{vt1} loss-of-function allele contains a seven base pair deletion that results in frame shift and premature stop codon (Ma et al., 2020b). Animals used for live imaging were in homozygous *nacre* (*mitfa*) mutant background to prevent pigment formation (Lister et al., 1999). The microglia RFP line [*Tg(mpeg1:Gal4;UAS:NTR-mCherry)*] was obtained from Dr. John Rawls at Duke University (Espenschied et al., 2019). The *crhb:LoxP-RFP-LoxP-GFP* line was generated using CRISPR-mediated knock-in, as described by Kimura et al. (Kimura et al., 2014). The sgRNA sequence for the *crhb* knock-in locus is AGC TCGCGTCTGCGCAGAG. All group-wise comparisons (mutants versus controls) were done between siblings.

RNA-seq and differential gene expression analysis

Progenies from heterozygous *dscaml1* mutant parents were anesthetized and harvested at 3.5-4 dpf. The anterior half of the animal was used for RNA preparation using the RNA Miniprep Kit (Zymo). The posterior half was used for genotyping. Three biological replicates for each group were analyzed, each containing RNA from 6–11 animals. All samples had RIN ≥8.0 and were converted into a strand-specific library using Illumina's TruSeq Stranded mRNA HT Sample Prep Kit (RS-122–2,103; Illumina) for subsequent cluster generation and sequencing on Illumina's NextSeq 75 sequencer. Sequence data processing, alignment, read count, mapping, and quality control were performed as previously described (Ates et al., 2020). Differential expression was tested for significance using the false discovery rate (FDR) (Benjamini–Hochberg) corrected Likelihood Ratio Test (LRT) in the R-package DESeq2 (Love et al., 2014). 238 and 116 genes showed a significant difference in read counts at FDR < 0.01 and 0.001, respectively. Original sequence data have been deposited in NCBI's Gene Expression Omnibus (Edgar et al., 2002) and accessible through GEO Series accession number GSE213858.

Fluorescent *in situ* hybridization and immunohistochemistry

Single and double whole-mount fluorescent *in situ* hybridization (FISH) was performed using protocols described previously (Pan et al., 2012). Probes were synthesized by *in vitro* transcription using the DIG and Fluorescein RNA Labeling Mix (Roche). DIG and fluorescein-labeled probes were detected with anti-DIG or anti-Fluorescein POD-conjugated Fab fragments (Roche) and Cy3 or Fluorescein TSA-plus Reagent (Akoya Biosciences). Plasmid template for *crhb* (Lohr et al., 2009) was provided by Dr. David Prober at Caltech. The *dscaml1* probe was generated as described previously (Ma et al., 2020b).

Immunohistochemistry was performed as described previously (Ma et al., 2020a). ERK1/2 was stained with mouse anti-ERK1/2 (4696S; Cell Signaling Technology). Activated caspase three was stained with rabbit anti-cleaved caspase 3 (559565; BD Biosciences). Nuclei were stained with TOTO-3 Iodide (ThermoFisher). RFP was stained with chicken anti-RFP (600-901-379S, Rockland) or rabbit anti-RFP (PM005, MBL Life Science). GFP was stained with rabbit anti-GFP (598, MBL Life Science). CRH was stained with rabbit anti-CRH (PBL rC68) provided by P. Sawchenko and J. Vaughan from the Salk Institute. All FISH and immunohistochemistry samples were mounted in 1.5% low-melt agarose in glass-bottomed Petri dishes (P50G-1.5–14-F; MatTek) and imaged using a Nikon A1 upright confocal microscope.

Cortisol extraction and ELISA

A detailed protocol for cortisol extraction and ELISA is provided online (Supplementary Datasheet S4). At 4.5 dpf, *dscaml1−/−* and control animals were separated based on the darker pigmentation of the *dscaml1−/−* animal (Ma et al., 2020b). 30–35 animals were placed in each petri dish for cortisol extraction. The morning baseline (unstressed) sample collections were done at 15–30 min after light onset (08:15–08:45), and the afternoon sample collections were done between 14:30–16:00. Hyperosmotic stress and stirring stress experiments were done between 14:30–15:30. 6 biological duplicates—each containing a pool of 30 animals—were collected for each genotype (*dscaml1−/−* and control) and stress condition (morning baseline, afternoon baseline, stirring stress, osmotic stress). Mutants and control animals are tested side by side for each experiment.

Stirring stress was induced by creating a vortex water flow with a spinning magnetic stir bar (Castillo-Ramirez et al., 2019). A small magnetic stir bar was placed into a 100 mm petri dish containing 35 animals and 20 mL of E3 media. The stir bar was rotated at 300 rpm with a stirring microplate for 5 min. Hyperosmotic stress was induced by increasing salt concentration in the media (Yeh et al., 2013). 30 animals were placed in 8 mL of E3 media. Then, 2 mL of prewarmed 1.25 M NaCl was added to the media for a final concentration of 250 mM for 20 min.

Sample homogenization and cortisol extraction were performed as described by Yeh et al. (Yeh et al., 2013). Briefly, 5 dpf larvae were rapidly immobilized with ice-cold E3 media and then flash-frozen at −80°C. Once all samples were collected, cortisol from the frozen samples was extracted with ethyl acetate (33211-1L-R; Sigma-Aldrich). Cortisol concentration was measured using a commercial ELISA kit, following the manufacturer's instructions (500360; Cayman Chemical). Sample plates were read with a microplate reader (FilterMax F3; MicroDevices) 90–120 min after initial development.

Live imaging of CRH neurons

Cre-mediated recombination of the *crhb:LRLG* transgene was induced by injecting Cre mRNA into the embryo at the 1-cell stage. To achieve partial Cre-mediated recombination, ~30 pg of CreER mRNA was injected at the 1-cell stage and 4-Hydroxytamoxifen (4-OHT) was added to the embryo media at 6 hpf (10 μM), followed by washout with E3 media at 24 hpf. To achieve complete Cre-mediated recombination, ~50 pg of *in vitro* transcribed Cre. zf1 mRNA (#61391, Addgene) was injected into the embryos (Horstick et al., 2015).

To perform confocal live imaging, 3 dpf animals were anesthetized with 0.01% tricaine methanesulfonate (MS-222, Sigma) and embedded in 1% low-melting point agarose, with the dorsal side resting on the glass surface inside the glass-bottomed petri dish (P50G-1.5–14-F; MatTek) (Beier et al., 2016). The petri dish was then filled with E3 media containing 0.01% tricaine methanesulfonate (MS-222, Sigma). Confocal z-stacks were acquired every 15 or 30 min for 12 h on a Nikon A1 confocal microscope.

Two-photon live imaging was done on a custom Bruker two-channel two-photon microscope. A tuneable Ti:Saphire laser (Chameleon Vision II; Coherent) was tuned to 980 nm to excite RFP and GFP simultaneously. 78 hpf animals were anesthetized and embedded the same way as confocal live imaging, but with the dorsal side away from the cover glass. Each animal was imaged at 78, 84, 96, 108, and 120 hpf (Figure 6A). After each time point, imaged larvae were gently removed from the agarose and recovered in E3 media at 28.5°C under normal day/night cycles. After the last time point, genomic DNA was prepared for all imaged animals and genotyped.

Image processing and statistical analyses

Images were processed using Fiji—an open-source image processing software (Schindelin et al., 2012). For FISH images, images were convolved (kernel = 12) to enhance cell boundaries, and the center of each cell was manually tagged using the ROI manager tool. The cell number equals the number of ROIs in each animal. The signal intensity per cell was defined as the median signal intensity of all ROIs in a given animal. The number of RFP+ cells in *crhb:LRLG* animals were counted using the ROI manager tool without convolution. For confocal live imaging, images were pre-processed using the Denoise. AI function in the Nikon Elements software. For two-photon imaging, z-stacks from different time points were aligned using the "Correct 3D drift" function. Spectral overlap between the RFP and GFP channels was linearly unmixed. Individual cells were tracked with the MTrackJ plugin in Fiji (Meijering et al., 2012).

All statistical analyses were performed in GraphPad Prism (Version 9). For normally-distributed data, parametric tests (*t*-test or ANOVA) were used. For non-normally distributed data, non-parametric tests (Mann-Whitney) were used. The Holm-Sidak post-test was used to correct for multiple comparisons, and the adjusted p values are shown. All values are expressed as mean ± standard error, unless otherwise noted. Statistical tests were considered significant when $p < 0.05$.

Quantification of apoptotic (AC3+) cells was done by the MAP-map quantitation and Z-Brain annotation method, but Anti-AC3 was used in place of anti-phosphorylated ERK1/2 (Randlett et al., 2015; Brunal et al., 2020). All MAP-map processing procedures (e.g., CMTK, MATLAB scripts) were performed as described by Randlett et al. The NPO is not annotated as such in Z-Brain, but the "Diencephalon - Otpb Cluster 2" ROI fits the definition of the NPO, as it delineate the dorsal region of the preoptic area that expresses *otpb* (Herget et al., 2014).

Data availability statement

Next-generation sequencing data utilized in this publication are available from the Gene Expression Omnibus (accession code GSE213858). All other data related to this study will be provided by the authors upon reasonable request.

Ethics statement

All procedures were performed according to protocols approved by the Institutional Animal Care and Use Committee at Virginia Tech and the National Institute for Basic Biology.

Author contributions

All authors contributed to the article and approved the submitted version. MM and YAP conceived and designed the experiments. MM and AAB prepared samples for RNA sequencing. YAP analyzed the RNA sequencing data. MM performed ELISA and histochemistry experiments and analyzed the data. MM and KCC performed *in situ* hybridization experiments and analyzed the data with contributions from CS and KS. SH generated the *crhbl:LRLG* transgenic line. MM and YAP wrote the manuscript. YAP provided project administration and acquired funding.

Funding

This work was supported by the Commonwealth Research Commercialization Fund (ER14S-001LS to YAP), the Virginia-Maryland College of Veterinary Medicine Intramural Research Fund, the Commonwealth Health Research Board Grant (#208–06-21 to YAP), the National Institutes of Health (R01MH131820), and funding from Virginia Tech.

Acknowledgments

We thank the animal care staff and veterinarians for animal husbandry; members of the Pan laboratory for helpful discussions; R. Settlage for computational analysis of RNA-seq data; S. Ryu and C. Yeh for sharing unpublished data; S. Imani for help with the quantification of IHC data; M. Wagle and S. Guo for advice on cortisol extraction procedures; M. Fox and A. Morozov for constructive feedback on the manuscript.

Conflict of interest

The authors declare that the research was conducted in the absence of any commercial or financial relationships that could be construed as a potential conflict of interest.

Publisher's note

Supplementary material

The Supplementary Material for this article can be found online at: https://www.frontiersin.org/articles/10.3389/fcell.2023.1113675/full#supplementary-material

SUPPLEMENTARY VIDEO S1
Time-lapse movie of *crhb:LRLG* larvae. CRH neurons were labeled with RFP (magenta) and GFP (green). Two cells (arrowheads, one green and one magenta), the same ones as shown in Figures 3H–H", move away over time.

SUPPLEMENTARY VIDEO S2
Time-lapse movie of larvae with CRH neurons labeled with GFP (green) and microglia labeled with mCherry (magenta). The red "X" marks the cell indicated in Figures 3I–J'. Maximum projection of z-stack for each time point is shown.

References

Alderman, S. L., and Bernier, N. J. (2009). Ontogeny of the corticotropin-releasing factor system in zebrafish. *Gen. Comp. Endocrinol.* 164, 61–69. doi:10.1016/j.ygcen.2009.04.007

Alsop, D., and Vijayan, M. (2009). The zebrafish stress axis: molecular fallout from the teleost-specific genome duplication event. *Gen. Comp. Endocrinol.* 161, 62–66. doi:10.1016/j.ygcen.2008.09.011

Alsop, D., and Vijayan, M. M. (2008). Development of the corticosteroid stress axis and receptor expression in zebrafish. *Am. J. Physiol. Regul. Integr. Comp. Physiol.* 294, R711–R719. doi:10.1152/ajpregu.00671.2007

Alvarez-Bolado, G. (2019). Development of neuroendocrine neurons in the mammalian hypothalamus. *Cell Tissue Res.* 375, 23–39. doi:10.1007/s00441-018-2859-1

Arnett, M. G., Muglia, L. M., Laryea, G., and Muglia, L. J. (2016). Genetic approaches to hypothalamic-pituitary-adrenal Axis regulation. *Neuropsychopharmacology* 41, 245–260. doi:10.1038/npp.2015.215

Ates, K. M., Wang, T., Moreland, T., Veeranan-Karmegam, R., Ma, M., Jeter, C., et al. (2020). Deficiency in the endocytic adaptor proteins PHETA1/2 impairs renal and craniofacial development. *Dis. models Mech.* 13, dmm041913. doi:10.1242/dmm.041913

Bai, Y., Liu, H., Huang, B., Wagle, M., and Guo, S. (2016). Identification of environmental stressors and validation of light preference as a measure of anxiety in larval zebrafish. *BMC Neurosci.* 17, 63. doi:10.1186/s12868-016-0298-z

Barton, B. A., Schreck, C. B., and Barton, L. D. (1987). Effects of chronic cortisol administration and daily acute stress on growth, physiological conditions, and stress responses in juvenile rainbow trout. *Dis. aquatic Org.* 2, 173–185. doi:10.3354/dao002173

Beier, K. T., Mundell, N. A., Pan, Y. A., and Cepko, C. L. (2016). Anterograde or retrograde transsynaptic circuit tracing in vertebrates with vesicular stomatitis virus vectors. *Curr. Protoc. Neurosci.* 74, 1.26.1–1.26.27. doi:10.1002/0471142301.ns0126s74

Brunal, A. A., Clark, K. C., Ma, M., Woods, I. G., and Pan, Y. A. (2020). Effects of constitutive and acute connexin 36 deficiency on brain-wide susceptibility to PTZ-induced neuronal hyperactivity. *Front. Mol. Neurosci.* 13, 587978. doi:10.3389/fnmol.2020.587978

Caramillo, E. M., Khan, K. M., Collier, A. D., and Echevarria, D. J. (2015). Modeling PTSD in the zebrafish: are we there yet? *Behav. Brain Res.* 276, 151–160. doi:10.1016/j.bbr.2014.05.005

Castillo-Ramirez, L. A., Ryu, S., and De Marco, R. J. (2019). Active behaviour during early development shapes glucocorticoid reactivity. *Sci. Rep.* 9, 12796. doi:10.1038/s41598-019-49388-3

Chandrasekar, G., Lauter, G., and Hauptmann, G. (2007). Distribution of corticotropin-releasing hormone in the developing zebrafish brain. *J. Comp. Neurol.* 505, 337–351. doi:10.1002/cne.21496

Clark, K. J., Boczek, N. J., and Ekker, S. C. (2011). Stressing zebrafish for behavioral genetics. *Rev. Neurosci.* 22, 49–62. doi:10.1515/RNS.2011.007

Cole, L. K., and Ross, L. S. (2001). Apoptosis in the developing zebrafish embryo. *Dev. Biol.* 240, 123–142. doi:10.1006/dbio.2001.0432

Dallman, M. F., Akana, S. F., Scribner, K. A., Bradbury, M. J., Walker, C. D., Strack, A. M., et al. (1992). Stress, feedback and facilitation in the hypothalamo-pituitary-adrenal Axis. *J. Neuroendocrinol.* 4, 517–526. doi:10.1111/j.1365-2826.1992.tb00200.x

Denver, R. J. (2009). Structural and functional evolution of vertebrate neuroendocrine stress systems. *Ann. N. Y. Acad. Sci.* 1163, 1–16. doi:10.1111/j.1749-6632.2009.04433.x

Edgar, R., Domrachev, M., and Lash, A. E. (2002). Gene Expression Omnibus: NCBI gene expression and hybridization array data repository. *Nucleic Acids Res.* 30 (1), 207–210. doi:10.1093/nar/30.1.207

Espenschied, S. T., Cronan Mark, R., Matty Molly, A., Mueller, O., Redinbo Matthew, R., Tobin David, M., et al. (2019). Epithelial delamination is protective during pharmaceutical-induced enteropathy. *Proc. Natl. Acad. Sci.* 116, 16961–16970. doi:10.1073/pnas.1902596116

Forger, N. G. (2009). Control of cell number in the sexually dimorphic brain and spinal cord. *J. Neuroendocrinol.* 21, 393–399. doi:10.1111/j.1365-2826.2009.01825.x

Fuerst, P. G., Bruce, F., Rounds, R. P., Erskine, L., and Burgess, R. W. (2012). Cell autonomy of DSCAM function in retinal development. *Dev. Biol.* 361, 326–337. doi:10.1016/j.ydbio.2011.10.028

Fuerst, P. G., Bruce, F., Tian, M., Wei, W., Elstrott, J., Feller, M. B., et al. (2009). DSCAM and DSCAML1 function in self-avoidance in multiple cell types in the developing mouse retina. *Neuron* 64, 484–497. doi:10.1016/j.neuron.2009.09.027

Garrett, A. M., Tadenev, A. L., and Burgess, R. W. (2012). DSCAMs: restoring balance to developmental forces. *Front. Mol. Neurosci.* 5, 86. doi:10.3389/fnmol.2012.00086

Garrett, A. M., Tadenev, A. L., Hammond, Y. T., Fuerst, P. G., and Burgess, R. W. (2016). Replacing the PDZ-interacting C-termini of DSCAM and DSCAML1 with epitope tags causes different phenotypic severity in different cell populations. *eLife* 5, e16144. doi:10.7554/eLife.16144

Griffiths, B. B., Schoonheim, P. J., Ziv, L., Voelker, L., Baier, H., and Gahtan, E. (2012). A zebrafish model of glucocorticoid resistance shows serotonergic modulation of the stress response. *Front. Behav. Neurosci.* 6, 68. doi:10.3389/fnbeh.2012.00068

Gutierrez-Triana, J. A., Herget, U., Castillo-Ramirez, L. A., Lutz, M., Yeh, C. M., De Marco, R. J., et al. (2015). Manipulation of interrenal cell function in developing zebrafish using genetically targeted ablation and an optogenetic tool. *Endocrinology* 156, 3394–3401. doi:10.1210/EN.2015-1021

Hayase, Y., Amano, S., Hashizume, K., Tominaga, T., Miyamoto, H., Kanno, Y., et al. (2020). Down syndrome cell adhesion molecule like-1 (DSCAML1) links the GABA system and seizure susceptibility. *Acta Neuropathol. Commun.* 8, 206. doi:10.1186/s40478-020-01082-6

Heap, L. A., Vanwalleghem, G. C., Thompson, A. W., Favre-Bulle, I., Rubinsztein-Dunlop, H., and Scott, E. K. (2017). Hypothalamic projections to the optic tectum in larval zebrafish. *Front. Neuroanat.* 11, 135. doi:10.3389/fnana.2017.00135

Herget, U., and Ryu, S. (2015). Coexpression analysis of nine neuropeptides in the neurosecretory preoptic area of larval zebrafish. *Front. Neuroanat.* 9, 2. doi:10.3389/fnana.2015.00002

Herget, U., Wolf, A., Wullimann, M. F., and Ryu, S. (2014). Molecular neuroanatomy and chemoarchitecture of the neurosecretory preoptic-hypothalamic area in zebrafish larvae. *J. Comp. Neurol.* 522, 1542–1564. doi:10.1002/cne.23480

Herman, J. P., and Tasker, J. G. (2016). Paraventricular hypothalamic mechanisms of chronic stress adaptation. *Front. Endocrinol.* 7, 137. doi:10.3389/fendo.2016.00137

Hooper, A., Paracha, R., and Maguire, J. (2018). Seizure-induced activation of the HPA axis increases seizure frequency and comorbid depression-like behaviors. *Epilepsy Behav. E&B* 78, 124–133. doi:10.1016/j.yebeh.2017.10.025

Horstick, E. J., Jordan, D. C., Bergeron, S. A., Tabor, K. M., Serpe, M., Feldman, B., et al. (2015). Increased functional protein expression using nucleotide sequence features enriched in highly expressed genes in zebrafish. *Nucleic acids Res.* 43, e48. doi:10.1093/nar/gkv035

Iossifov, I., O'Roak, B. J., Sanders, S. J., Ronemus, M., Krumm, N., Levy, D., et al. (2014). The contribution of de novo coding mutations to autism spectrum disorder. *Nature* 515, 216–221. doi:10.1038/nature13908

Irles, C., Nava-Kopp, A. T., Morán, J., and Zhang, L. (2014). Neonatal maternal separation up-regulates protein signalling for cell survival in rat hypothalamus. *Stress* 17, 275–284. doi:10.3109/10253890.2014.913017

Johnson, S. A., Fournier, N. M., and Kalynchuk, L. E. (2006). Effect of different doses of corticosterone on depression-like behavior and HPA axis responses to a novel stressor. *Behav. Brain Res.* 168, 280–288. doi:10.1016/j.bbr.2005.11.019

Karaca, E., Harel, T., Pehlivan, D., Jhangiani, S. N., Gambin, T., Coban Akdemir, Z., et al. (2015). Genes that affect brain structure and function identified by rare variant analyses of mendelian neurologic disease. *Neuron* 88, 499–513. doi:10.1016/j.neuron.2015.09.048

Keen-Rhinehart, E., Michopoulos, V., Toufexis, D. J., Martin, E. I., Nair, H., Ressler, K. J., et al. (2009). Continuous expression of corticotropin-releasing factor in the central nucleus of the amygdala emulates the dysregulation of the stress and reproductive axes. *Mol. Psychiatry* 14, 37–50. doi:10.1038/mp.2008.91

Kimura, Y., Hisano, Y., Kawahara, A., and Higashijima, S. (2014). Efficient generation of knock-in transgenic zebrafish carrying reporter/driver genes by CRISPR/Cas9-mediated genome engineering. *Sci. Rep.* 4, 6545. doi:10.1038/srep06545

Kolber, B. J., Boyle, M. P., Wieczorek, L., Kelley, C. L., Onwuzurike, C. C., Nettles, S. A., et al. (2010). Transient early-life forebrain corticotropin-releasing hormone elevation causes long-lasting anxiogenic and despair-like changes in mice. *J. Neurosci.* 30, 2571–2581. doi:10.1523/JNEUROSCI.4470-09.2010

Lister, J. A., Robertson, C. P., Lepage, T., Johnson, S. L., and Raible, D. W. (1999). Nacre encodes a zebrafish microphthalmia-related protein that regulates neural-crest-derived pigment cell fate. *Development* 126, 3757–3767. doi:10.1242/dev.126.17.3757

Lohr, H., and Hammerschmidt, M. (2011). Zebrafish in endocrine systems: recent advances and implications for human disease. *Annu. Rev. Physiol.* 73, 183–211. doi:10.1146/annurev-physiol-012110-142320

Lohr, H., Ryu, S., and Driever, W. (2009). Zebrafish diencephalic A11-related dopaminergic neurons share a conserved transcriptional network with neuroendocrine cell lineages. *Development* 136, 1007–1017. doi:10.1242/dev.033878

Love, M. I., Huber, W., and Anders, S. (2014). Moderated estimation of fold change and dispersion for RNA-seq data with DESeq2. *Genome Biol.* 15, 550. doi:10.1186/s13059-014-0550-8

Ma, M., Kler, S., and Pan, Y. A. (2020a). Structural neural connectivity analysis in zebrafish with restricted anterograde transneuronal viral labeling and quantitative brain mapping. *Front. Neural circuits* 13, 85. doi:10.3389/fncir.2019.00085

Ma, M., Ramirez, A. D., Wang, T., Roberts, R. L., Harmon, K. E., Schoppik, D., et al. (2020b). Zebrafish *dscaml1* deficiency impairs retinal patterning and oculomotor function. *J. Neurosci.* 40, 143–158. doi:10.1523/JNEUROSCI.1783-19.2019

Maack, G., and Segner, H. (2003). Morphological development of the gonads in zebrafish. *J. Fish Biol.* 62, 895–906. doi:10.1046/j.1095-8649.2003.00074.x

Mazaheri, F., Breus, O., Durdu, S., Haas, P., Wittbrodt, J., Gilmour, D., et al. (2014). Distinct roles for BAI1 and TIM-4 in the engulfment of dying neurons by microglia. *Nat. Commun.* 5, 4046. doi:10.1038/ncomms5046

McEwen, B. S., and Akil, H. (2020). Revisiting the stress concept: Implications for affective disorders. *J. Neurosci.* 40, 12–21. doi:10.1523/JNEUROSCI.0733-19.2019

Meijering, E., Dzyubachyk, O., and Smal, I. (2012). Methods for cell and particle tracking. *Methods Enzymol.* 504, 183–200. doi:10.1016/B978-0-12-391857-4.00009-4

Mi, H., Ebert, D., Muruganujan, A., Mills, C., Albou, L-P., Mushayamaha, T., et al. (2021). PANTHER version 16: a revised family classification, tree-based classification tool, enhancer regions and extensive API. *Nucleic Acids Res.* 49, D394–D403. doi:10.1093/nar/gkaa1106

Moreland, T., and Poulain, F. E. (2022). To stick or not to stick: The multiple roles of cell adhesion molecules in neural circuit assembly. *Front. Neurosci.* 16, 889155. doi:10.3389/fnins.2022.889155

Muto, A., Taylor, M. R., Suzawa, M., Korenbrot, J. I., and Baier, H. (2013). Glucocorticoid receptor activity regulates light adaptation in the zebrafish retina. *Front. Neural Circuits* 7, 145. doi:10.3389/fncir.2013.00145

Nagpal, J., Herget, U., Choi, M. K., and Ryu, S. (2019). Anatomy, development, and plasticity of the neurosecretory hypothalamus in zebrafish. *Cell Tissue Res.* 375, 5–22. doi:10.1007/s00441-018-2900-4

Nüsslein-Volhard, C., Gilmour, D., and Dahm, R. (2002). "Introduction: zebrafish as a system to study development and organogenesis," in *Zebrafish: A practical approach*, 1–5.

O'Toole, K. K., Hooper, A., Wakefield, S., and Maguire, J. (2014). Seizure-induced disinhibition of the HPA axis increases seizure susceptibility. *Epilepsy Res.* 108, 29–43. doi:10.1016/j.eplepsyres.2013.10.013

Ogata, S., Hashizume, K., Hayase, Y., Kanno, Y., Hori, K., Balan, S., et al. (2021). Potential involvement of DSCAML1 mutations in neurodevelopmental disorders. *Genes Cells* 26, 136–151. doi:10.1111/gtc.12831

Pan, Y. A., Choy, M., Prober, D. A., and Schier, A. F. (2012). Robo2 determines subtype-specific axonal projections of trigeminal sensory neurons. *Development* 139, 591–600. doi:10.1242/dev.076588

Placzek, M., Fu, T., and Towers, M. (2020). "Development of the neuroendocrine hypothalamus," in *Developmental neuroendocrinology*. Editors S. Wray and S. Blackshaw (Cham: Springer International Publishing), 3–30.

Pyati, U. J., Gjini, E., Carbonneau, S., Lee, J. S., Guo, F., Jette, C. A., et al. (2011). p63 mediates an apoptotic response to pharmacological and disease-related ER stress in the developing epidermis. *Dev. Cell* 21, 492–505. doi:10.1016/j.devcel.2011.07.012

Randlett, O., Wee, C. L., Naumann, E. A., Nnaemeka, O., Schoppik, D., Fitzgerald, J. E., et al. (2015). Whole-brain activity mapping onto a zebrafish brain atlas. *Nat. Methods* 12, 1039–1046. doi:10.1038/nmeth.3581

Regev, L., and Baram, T. Z. (2014). Corticotropin releasing factor in neuroplasticity. *Front. Neuroendocrinol.* 35, 171–179. doi:10.1016/j.yfrne.2013.10.001

Saadatmand, F., Gurdziel, K., Jackson, L., Kwabi-Addo, B., and Ruden, D. M. (2021). DNA methylation and exposure to violence among African American young adult males. *Brain, Behav. Immun. - Health* 14, 100247. doi:10.1016/j.bbih.2021.100247

Sachse, S. M., Lievens, S., Ribeiro, L. F., Dascenco, D., Masschaele, D., Horre, K., et al. (2019). Nuclear import of the DSCAM-cytoplasmic domain drives signaling capable of inhibiting synapse formation. *EMBO J.* 38, e99669. doi:10.15252/embj.201899669

Sanes, J. R., and Zipursky, S. L. (2020). Synaptic specificity, recognition molecules, and assembly of neural circuits. *Cell* 181, 536–556. doi:10.1016/j.cell.2020.04.008

Schindelin, J., Arganda-Carreras, I., Frise, E., Kaynig, V., Longair, M., Pietzsch, T., et al. (2012). Fiji: an open-source platform for biological-image analysis. *Nat. Methods* 9, 676–682. doi:10.1038/nmeth.2019

Shainer, I., Kuehn, E., Laurell, E., Al Kassar, M., Mokayes, N., Sherman, S., et al. (2022). A single-cell resolution gene expression atlas of the larval zebrafish brain. *bioRxiv* [Preprint]. doi:10.1101/2022.02.11.479024

Simerly, R. B. (2002). Wired for reproduction: organization and development of sexually dimorphic circuits in the mammalian forebrain. *Annu. Rev. Neurosci.* 25, 507–536. doi:10.1146/annurev.neuro.25.112701.142745

Spencer, R. L., and Deak, T. (2017). A users guide to HPA axis research. *Physiol. Behav.* 178, 43–65. doi:10.1016/j.physbeh.2016.11.014

Stenzel-Poore, M. P., Cameron, V. A., Vaughan, J., Sawchenko, P. E., and Vale, W. (1992). Development of Cushing's syndrome in corticotropin-releasing factor transgenic mice. *Endocrinology* 130, 3378–3386. doi:10.1210/endo.130.6.1597149

Stroth, N., Holighaus, Y., Ait-Ali, D., and Eiden, L. E. (2011). PACAP: a master regulator of neuroendocrine stress circuits and the cellular stress response. *Ann. N. Y. Acad. Sci.* 1220, 49–59. doi:10.1111/j.1749-6632.2011.05904.x

Vom Berg-Maurer, C. M., Trivedi, C. A., Bollmann, J. H., De Marco, R. J., and Ryu, S. (2016). The severity of acute stress is represented by increased synchronous activity and recruitment of hypothalamic CRH neurons. *J. Neurosci.* 36, 3350–3362. doi:10.1523/JNEUROSCI.3390-15.2016

Wagle, M., Zarei, M., Lovett-Barron, M., Poston, K. T., Xu, J., Ramey, V., et al. (2022). Brain-wide perception of the emotional valence of light is regulated by distinct hypothalamic neurons. *Mol. Psychiatry* 27, 3777–3793. doi:10.1038/s41380-022-01567-x

Watts, A. G. (2005). Glucocorticoid regulation of peptide genes in neuroendocrine CRH neurons: A complexity beyond negative feedback. *Front. Neuroendocrinol.* 26, 109–130. doi:10.1016/j.yfrne.2005.09.001

Wendelaar Bonga, S. E. (1997). The stress response in fish. *Physiol. Rev.* 77, 591–625. doi:10.1152/physrev.1997.77.3.591

Wilson, C. A., High, S. K., McCluskey, B. M., Amores, A., Yan, Y. L., Titus, T. A., et al. (2014). Wild sex in zebrafish: loss of the natural sex determinant in domesticated strains. *Genetics* 198, 1291–1308. doi:10.1534/genetics.114.169284

Wong, F. K., and Marin, O. (2019). Developmental cell death in the cerebral cortex. *Annu. Rev. Cell Dev. Biol.* 35, 523–542. doi:10.1146/annurev-cellbio-100818-125204

Yamagata, M., and Sanes, J. R. (2008). Dscam and Sidekick proteins direct lamina-specific synaptic connections in vertebrate retina. *Nature* 451, 465–469. doi:10.1038/nature06469

Yamagata, M., and Sanes, J. R. (2010). Synaptic localization and function of Sidekick recognition molecules require MAGI scaffolding proteins. *J. Neurosci.* 30, 3579–3588. doi:10.1523/JNEUROSCI.6319-09.2010

Yamaguchi, Y., and Miura, M. (2015). Programmed cell death in neurodevelopment. *Dev. Cell* 32, 478–490. doi:10.1016/j.devcel.2015.01.019

Yeh, C. M., Glock, M., and Ryu, S. (2013). An optimized whole-body cortisol quantification method for assessing stress levels in larval zebrafish. *PLoS One* 8, e79406. doi:10.1371/journal.pone.0079406

Zhang, L., Hernández, V. S., Liu, B., Medina, M. P., Nava-Kopp, A. T., Irles, C., et al. (2012). Hypothalamic vasopressin system regulation by maternal separation: its impact on anxiety in rats. *Neuroscience* 215, 135–148. doi:10.1016/j.neuroscience.2012.03.046

Ziv, L., Muto, A., Schoonheim, P. J., Meijsing, S. H., Strasser, D., Ingraham, H. A., et al. (2013). An affective disorder in zebrafish with mutation of the glucocorticoid receptor. *Mol. Psychiatry* 18, 681–691. doi:10.1038/mp.2012.64